
Federated Distillation for Medical Image Classification: Towards Trustworthy Computer-Aided Diagnosis

Sufen Ren[†], Yule Hu[‡], Shengchao Chen[§], and Guanjun Wang^{††}

[†] School of Information and Communication Engineering, Hainan University, China

[‡] College of Mathematical Sciences, BoHai University, China

[§] Australian AI Institute, University of Technology Sydney, Australia

^{††} School of Electronic Science and Technology, Hainan University, China

Corresponding to: shengchao.chen.uts@gmail.com, wangguanjun@hainanu.edu.cn

Abstract

Medical image classification plays a crucial role in computer-aided clinical diagnosis. While deep learning techniques have significantly enhanced efficiency and reduced costs, the privacy-sensitive nature of medical imaging data complicates centralized storage and model training. Furthermore, low-resource healthcare organizations face challenges related to communication overhead and efficiency due to increasing data and model scales. This paper proposes a novel privacy-preserving medical image classification framework based on federated learning to address these issues, named FEDMIC. The framework enables healthcare organizations to learn from both global and local knowledge, enhancing local representation of private data despite statistical heterogeneity. It provides customized models for organizations with diverse data distributions while minimizing communication overhead and improving efficiency without compromising performance. Our FEDMIC enhances robustness and practical applicability under resource-constrained conditions. We demonstrate FEDMIC's effectiveness using four public medical image datasets for classical medical image classification tasks.

1 Introduction

Deep learning (DL)-based medical image classification (MIC) leverages computer vision techniques to automate the analysis and classification of extensive medical image dataset [Chen et al., 2023a]. Unlike traditional methods that depend on medical experts for multiple patient assessments [Shi et al., 2023], this technology offers significant advantages in disease prevention, diagnosis, treatment planning, and patient management, enhancing both the accuracy and efficiency of diagnoses [Li et al., 2023]. Currently, DL models rely on extensive labeled datasets to achieve high accuracy through increased model complexity. However, traditional centralized training approaches, which process all data on a central server, conflict with the practicalities of medical care, particularly concerning patient privacy and data security [Jiang et al., 2023]. Specifically, the transfer of patient data among healthcare providers is restricted by privacy and ethical regulations, limiting its use in centralized training. This restriction presents a significant challenge in developing efficient automated MIC models that can provide reliable support for clinical practice.

Existing related works based on advanced DL techniques mainly focus on improving through well-designed modules and learning strategies to optimize feature extraction capabilities [Chen et al., 2023a, Wang et al., 2024a, Li et al., 2023]. However, analyzing medical data using these methods via centralized cloud computing presents significant challenges in real-world applications. Specifically, these challenges include network dependency and privacy concerns:

Sufen Ren and Yule Hu contributed equally to this work.

- (i) **Network Dependency:** Healthcare organizations generate vast amounts of patient data daily. Transmitting this data to a central server imposes a substantial communication burden, which is impractical for healthcare organizations with limited resources.
- (ii) **Privacy Concerns:** Electronic medical records of different patients are often distributed across various healthcare organizations. Sharing patient data between organizations is typically subject to stringent medical privacy protection and ethical regulations.

These constraints make it difficult for organizations to access a full range of medical images, limiting their ability to conduct effective analysis and obtain reliable insights. To address these issues, on-device intelligence for analyzing medical image data directly on the devices is crucial, as it reduces the need for data transfers, protects privacy, and decreases reliance on networks.

Federated Learning (FL) [McMahan et al., 2017] is a promising paradigm for on-device intelligence that trains a uniform DL model collaboratively across multiple devices without revealing data. It is increasingly popular in healthcare [Dasaradharami Reddy et al., 2023, Li et al., 2023], recommendations [Imran et al., 2023, Zhang et al., 2023a,b], weather [Chen et al., 2023b,c], remote sensing [Zhai et al., 2023, Zhang et al., 2023c], and so on [Chen et al., 2023d, Ren et al., 2024]. Models trained by vanilla FL often underperform due to statistical heterogeneity, characterized by non-independent and identically distributed (Non.IID) data across devices. This challenge is exacerbated in federated MIC due to subtle inter-category differences and skewed data distribution among categories. These factors impede the training of a globally effective model. Developing strategies to enhance performance in the presence of significant statistical heterogeneity remains an open research challenge.

Shallow models often fail to capture the complex representations necessary for discerning key patient characteristics in medical images, including anatomical (shape and location of organs), pathological (masses and abnormal tissues), textural (grayscale distributions and localized texture patterns), and morphological features (edge sharpness and shape). While existing literature suggests adopting more complex structures to enhance model capabilities, this approach incurs higher computational costs [Huo et al., 2024, Chen et al., 2023a, Han et al., 2024]. These sophisticated models pose significant challenges for FL systems due to the frequent exchange of model updates between servers and clients—a process that becomes increasingly demanding with model complexity. This heightened communication burden is particularly problematic for resource-constrained devices in healthcare organizations.

To address these challenges, we propose a novel Personalized Federated Distillation for Medical Image Classification, dubbed FEDMIC. This approach targets cross-healthcare organization medical image classification tasks with distributed, heterogeneous data, facilitating collaborative model training across databases while allowing personalized models without raw data sharing. FEDMIC employs a Dual Knowledge Distillation (**Dual-KD**) strategy for local updating, enabling clients to develop custom local models that learn from both global and local knowledge without compromising privacy. Additionally, we introduce a Global Parameter Decomposition (**GPD**) method that compresses the full local inference model into low-rank matrices. By applying information entropy-based constraints, GPD filters out unnecessary parameters, significantly reducing communication costs while maintaining performance. This approach minimizes parameter transmission, making FedMIC suitable for low-resource environments.

We quantitatively evaluate the performance of the proposed FEDMIC and typical FL algorithms using four publicly available medical image classification datasets, including both 2D and 3D images. The main contributions of this work are:

- A privacy-preserving framework, FEDMIC, for cross-healthcare organization medical image classification tasks. This is the first solution to address the weak performance caused by the notorious heterogeneity while ensuring low communication costs.
- An effective dual knowledge distillation strategy within FEDMIC. This method enables each client’s student model to learn from both global and local knowledge while maintaining privacy, resulting in highly personalized models tailored to specific data distributions.
- A global parameter decomposition strategy during the aggregation process. This approach reduces communication overhead between clients and servers, improving efficiency by significantly decreasing transmission parameters while maintaining performance.

- Extensive experiments on four publicly available real-world medical image classification datasets, demonstrating that FEDMIC outperforms state-of-the-art FL algorithms and provides an efficient distributed learning strategy for low-resource scenarios.

2 Related Work

This section presents work related to our FEDMIC, including Deep Learning-based Medical Image Classification (**Section. 2.1**) and Privacy-Preserving Federated Learning (**Section. 2.2**).

2.1 Deep Learning-based Medical Image Classification

DL has substantially reduced automation costs across diverse applications [Chen et al., 2023e,f,g, Peng et al., 2023, Chen et al., 2022a,b]. In medical image classification, DL techniques provide a more reliable and cost-effective solution for clinical analysis support, eliminating the need for high labor expenditures. However, medical image classification presents unique challenges compared to the analysis of natural images, particularly in capturing complex representations such as anatomical, textural, and morphological features.

While deep networks have been used to extract features from large-scale medical image datasets, effectively obtaining useful representations is still difficult. Recent efforts have focused on designing sophisticated modules for improved performance. For instance, Chen et al. [Chen et al., 2023a] introduced a hierarchical attention mechanism that enhances the performance of Transformers in multi-label classification while reducing spatio-temporal complexity. Huo et al. [Huo et al., 2024] developed a three-branch hierarchical multi-scale feature fusion strategy that fuses global and local features without disrupting their modeling, thus improving efficiency. Han et al. [Han et al., 2024] proposed a dynamic multi-scale convolutional neural network with an uncertainty quantification strategy to accelerate model convergence on medical images. Wang et al. [Wang et al., 2024a,b] suggested an ensemble learning strategy using multiple models pretrained on natural images to enhance the representation of complex medical images. Despite these advances, current models often overlook privacy concerns and are limited by their large parameter sizes, making them unsuitable for low-resource scenarios. Our study addresses these issues by focusing on a method that prioritizes privacy without compromising performance, particularly in low-resource environments.

2.2 Privacy-Preserving Federated Learning

Federated Learning (FL) [McMahan et al., 2017] is a distributed machine learning paradigm that enables collaborative model training among multiple users without compromising data privacy. This approach has found applications in diverse fields, including recommendation systems [Neumann et al., 2023, Zhang et al., 2023b], climate change [Chen et al., 2023b,c, 2024], and healthcare [Rauniyar et al., 2023, Zhang et al., 2023d]. However, FL faces two primary challenges: statistical heterogeneity (Non-IID) and communication efficiency. This paper provides a concise overview of recent advancements in addressing these challenges within the FL framework.

Statistical Heterogeneity in FL Various FL algorithms employ regularization techniques to ensure convergence in the presence of statistical heterogeneity. Li et al. [Li et al., 2020] introduced a local regularization term to optimize individual client models, while Karimireddy et al. [Karimireddy et al., 2020] proposed a novel stochastic algorithm using control variates to address this challenge. Adaptations of Elastic Weight Consolidation (EWC) to FL scenarios have been explored by Shoham et al. [Shoham et al., 2019] and Yao et al. Yao and Sun [2020]. The former applied EWC to mitigate catastrophic forgetting during task transfer by selectively penalizing parameter vectors that deviate significantly from those learned in previous tasks. The latter utilized EWC to estimate the global model’s importance weight matrix and incorporate each client’s knowledge. Li et al. [Li et al., 2021a] expanded on this concept by implementing regularization between global and local models, as well as between current and previous local models. To handle non-IID data and enhance training stability, Xu et al. [Xu et al., 2022] developed an adaptive weighted proximal regularization term based on estimated noise levels. While effective, these methods often incur high computational costs when dealing with large-scale parameter regularization.

Personalized Federated Learning (PFL) offers a more effective solution to the non-IID challenge than regularization-based methods by enabling the development of client-specific models. Several approaches have been proposed in this domain. pFedMe employs Moreau envelopes to create a regularized local objective, facilitating the separation of personalized model optimization from global learning [T Dinh et al., 2020]. PerFedAvg, inspired by Model-Agnostic Meta-Learning, introduces a decentralized meta-learning framework to establish an initial model for rapid client adaptation [Fallah et al., 2020]. Although these approaches show promising results, most overlook the feature shift problem, with the notable exception of FedBN [Li et al., 2021b], which employs local batch normalization to mitigate this issue. Knowledge Distillation (KD)-based personalization techniques such as FedBE [Chen and Chao, 2021] also help diminish the effects of non-IID by refining global and local representations. FedMD [Li and Wang, 2019], for instance, promotes inter-client learning by using knowledge distillation and transfer learning to align each local model with the global consensus. However, these strategies typically rely on averaging to form this consensus, heavily dependent on the quality of public data. To reduce this dependency, ensemble distillation using generated data and compressed federated distillation techniques [Lin et al., 2020], which incorporate distilled data curation, soft-label quantization, and delta-encoding, have been developed to lower communication costs [Sattler et al., 2020]. Data-free knowledge distillation is another innovative approach where a server-derived lightweight generator [Zhu et al., 2021], built solely from client model predictions, is distributed to clients. This generator uses the aggregated knowledge as an inductive bias to guide local training.

Communication Efficiency in FL Heterogeneous environments can impair training efficiency. Consequently, enhancing communication efficiency and effectiveness has become a focal point in current efforts [Chen et al., 2023b,c, Bibikar et al., 2022]. Chen et al. [Chen et al., 2023b,c] introduced a few parameters as prompts independent from the training model, and only activated and transmitted prompts during training and communication to reduce the computational burden. However, training a limited number of parameters often leads to a trade-off between performance and efficiency. Yao et al. [Yao et al., 2019] reduces the number of communication rounds by integrating a maximum mean discrepancy constraint into the optimization objective. Dai et al. [Dai et al., 2022] implements a decentralized sparse training approach, allowing each local model to utilize a personalized sparse mask to identify active parameters, which remain consistent during local training and peer-to-peer communication. This method requires only the initial transmission of the indices of active parameters, followed by the transmission of their values in subsequent communications, thereby substantially lowering communication costs. In this paper, we propose FEDMIC, a parameter-efficient personalized method for federated medical image classification. FEDMIC aims to provide highly customized models for each client, improving learning in the face of heterogeneity while significantly reducing communication overhead between clients and the server.

3 Preliminaries

Federated Learning Under Vanilla FedAvg [McMahan et al., 2017], a central server coordinates N clients to collaboratively train a uniform global model intended to generalize across all devices. Specifically, in each communication round t , the server samples a fraction of all the clients, C , to join the training. The server distributes the global model w to these clients. Each selected client received global model on their private dataset $D_k - P_k$ (D_k obeys the distribution P_k) to obtain w_k through local training process $w_k \leftarrow w - \eta \nabla \ell(w; x_i, y_i), (x_i, y_i) \in D_k$. The k -th client uploads the trained local model w_k to the server that aggregates them to update the global model via $w = \sum_{k=0}^{K-1} \frac{n_k}{n} w_k$. FedAvg aims to minimize the average loss of the global model w on all clients' local datasets:

$$F(w) := \arg \min_{w_1, w_2, \dots, w_N} \sum_{k=1}^N \frac{n_k}{n} F_k(w_k) \quad (1)$$

where n_k is the number of samples stored by the k -th client. n is the number of samples held by all clients. $F_k(w_k)$ denotes the local objective function of k -th client that can be formulated as $\mathcal{L}_k(w_k) = \ell_k(w_k; (x_i, y_i))$, where the \mathcal{L} is loss function.

Problem Formulation for FedMIC The core framework of our proposed FEDMIC aligns with the standard FedAvg protocol, with key distinctions in data distribution and resource constraints. In

FEDMIC, each client possesses a unique distribution of medical image data, creating a statistically heterogeneous environment. Moreover, healthcare organizations typically operate with limited computational resources, facing challenges in managing large-scale data and complex neural networks. This setup reflects real-world constraints in storage, communication, and processing capabilities. Consequently, FEDMIC addresses two primary challenges: (1) *mitigating the impact of statistical heterogeneity on Federated Medical Image Classification* and (2) *reducing communication overhead and enhancing efficiency without compromising model effectiveness*.

4 Methodology

This section elaborates on the details of our proposed framework, FEDMIC. This section is divided into three parts, including (1) Framework Architecture of FEDMIC (**Section. 4.1**), (2) Dual Knowledge Distillation (Dual-KD) (**Section. 4.2**), and (3) Global Parameter Decomposition (GPD) (**Section. 4.3**).

4.1 Framework Architecture of FEDMIC

Architecture of our FEDMIC is as shown in Figure 1, which comprising N clients denote different healthcare organization, and a central server. Each client maintains two local model, a local teacher model and a local student model, which is work during inference, while the teacher model does not work during inference. In addition, each client does not share any local data during training, thus ensuring the privacy of each health organization. The central server does not access any client’s data.

In contrast to FedAvg [McMahan et al., 2017], FEDMIC employs a dual-model approach where clients update both a local student model and a local teacher model during each global communication round. However, only the student model parameters are transmitted to the server, while the teacher model remains local, facilitating personalized knowledge distillation. The server aggregates the received student model parameters and disseminates the updated model to all clients for the subsequent communication round. This iterative process continues until the student model converges. Unlike traditional centralized training methods, this approach eliminates the need for raw data sharing, significantly reducing the transmission of sensitive information. Consequently, the framework enhances privacy protection for participating healthcare organizations during model training.

4.2 Dual Knowledge Distillation Mechanism on Local Updating

Knowledge Distillation (KD) enables simpler models to learn from more complex ones, enhancing their performance through knowledge transfer [Habib et al., 2023]. In real-world medical applications, data heterogeneity among healthcare organizations poses significant challenges, rendering global models ineffective across diverse data distributions. To address this Non-IID challenge and its negative impact on model performance, we propose a novel KD strategy within FedMIC, termed Dual Knowledge Distillation (Dual-KD). Unlike traditional KD approaches that focus on local parameter reduction or global-to-local model distillation, our Dual-KD encourages student models to integrate insights from both local and global knowledge, bridging the gap between local and global representations.

The local updating process within FEDMIC is shown in Figure 2. Dual-KD employs two structurally consistent networks: a teacher model and a student model. During local updates, both models learn concurrently from local medical imaging data. Crucially, only the student model’s parameters are uploaded to the server for global collaborative learning, enabling it to incorporate global knowledge. The teacher model, updated locally, enhances its capacity for personalized learning based on local data. Dual-KD facilitates mutual learning between the models; the student model benefits from acquired global insights, while the teacher model develops robust, personalized representations. This approach not only tailors local models to the specific needs of Non-IID clients but also facilitates global knowledge sharing without compromising privacy, thereby preventing data silos.

To enhance knowledge transfer between local teacher models and student models, which includes both locally personalized knowledge and insights aimed at global understanding, we introduce two distinct local optimization objectives within our Dual-KD strategy: Representation Distillation Loss (RDL, \mathcal{L}_{rep}) and Decision Distillation Loss (DDL, \mathcal{L}_{dec}). The former is used to align the potential representations from teacher and student models, and the latter is used correct each other between

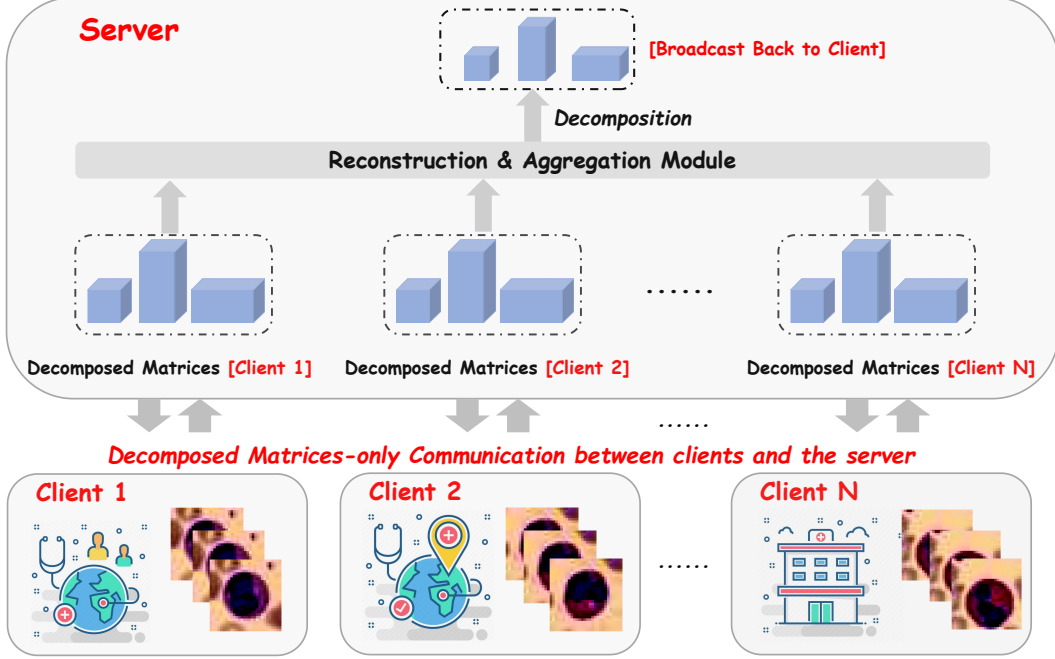


Figure 1: Schematic diagram of our FEDMIC. Each healthcare organization as an independent client with private medical images that remain unshared throughout the training process. Clients train their local models using exclusively local data before transmitting parameters to the central server. FedMIC significantly reduces communication overhead by transmitting only a small subset of parameters from the decomposition matrix, rather than the entire local model. The server reconstructs and aggregates these uploaded parameters within its service area, subsequently broadcasting the aggregated parameters to all clients for the next iteration of training and communication.

classification decisions on potential representations of medical images. For these objectives, we divide both the teacher and student models into two components: the Backbone, responsible for data representation extraction, and the Head, which acts as a classifier utilizing these representations to make decisions. The local medical images on client i is labeled as \mathbf{X}_i , with the predictions from the local teacher and student models denoted as \mathbf{Y}_i^t and \mathbf{Y}_i^s , respectively. To counteract potential performance degradation due to misleading backbone representations, we introduce a trainable auxiliary matrix \mathbf{W}_{aux} . This matrix ensures accurate updates to both models, facilitating bidirectional corrections. The process of extracting representations is described as follows:

$$\mathbf{H}_{hs}^s = \text{Backbone}^s(\mathbf{X}_i), \quad \mathbf{H}_{hs}^t = \text{Backbone}^t(\mathbf{X}_i), \quad (2)$$

where the Backbone^s and Backbone^t denote the backbone of the teacher and the student model, respectively. Then the process of dual-way correction (Representation Distillation Loss in Figure 2) can be formulated as:

$$\mathcal{L}_{rep} = \frac{1}{n} \sum_{i=1}^n (\mathbf{H}_{hs}^s \cdot \mathbf{W}_{aux} - \mathbf{H}_{hs}^t \cdot \mathbf{W}_{aux})^2. \quad (3)$$

To construct the above-mentioned Decision Distillation Loss, we use the target label to compute the task losses for both the teacher model and the student model. Task losses for these two models can be formulated based on standard Cross-Entropy Loss:

$$\mathcal{L}_{task}^t = - \sum_i \mathbf{Y}_i^t \log(\mathbf{Y}), \quad \mathcal{L}_{task}^s = - \sum_i \mathbf{Y}_i^s \log(\mathbf{Y}), \quad (4)$$

where the \mathbf{Y} is the distribution of ground truth of local label, \mathbf{Y}_i^t and \mathbf{Y}_i^s can be expressed as $\text{Head}^s(\mathbf{H}_{hs}^s)$ and $\text{Head}^t(\mathbf{H}_{hs}^s)$ according to the above-mentioned Backbone-Head setting. The DDL consists of two part: representation-based part and decision-based part, for achieving comprehensive

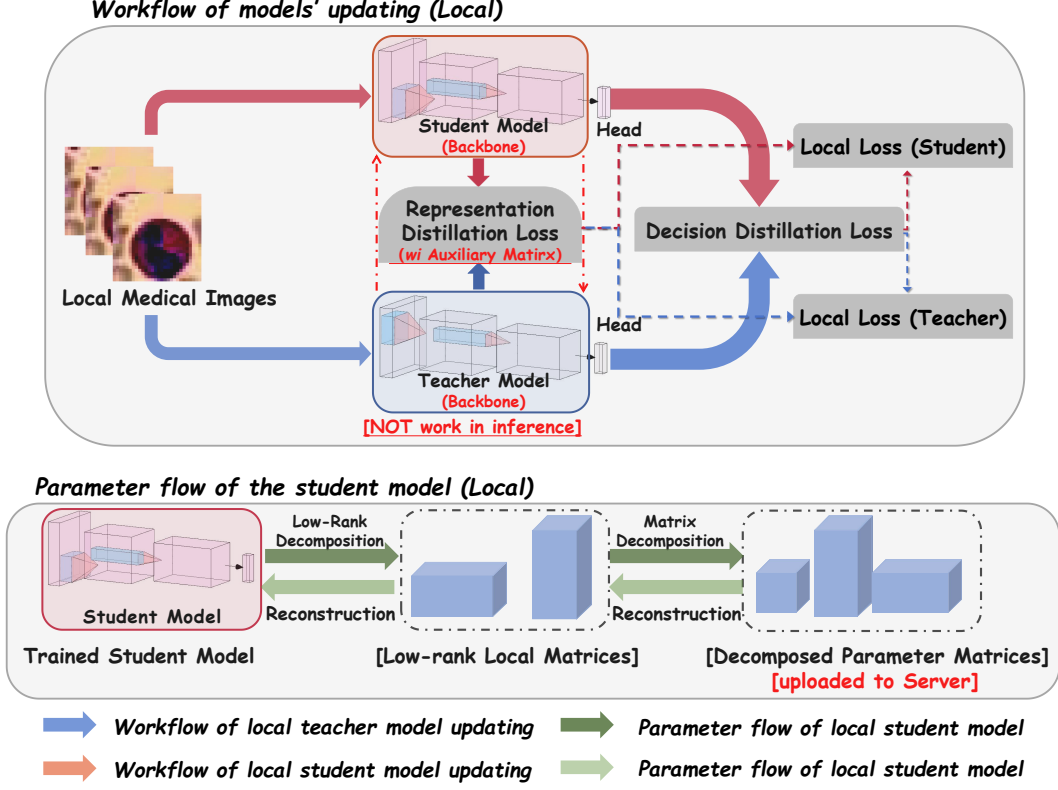


Figure 2: Schematic diagram of the process of local updating within our FEDMIC. The local update comprises two primary phases: (1) local model updating and (2) parameter flow of the updated local model. In phase one, duplicate local medical image data are input into both student and teacher models. The extracted representations are used to compute the representational distillation loss, facilitating bi-directional correction. These representations are then fed into the corresponding model heads for decision-making, where the decision distillation loss is calculated using two independent auxiliary matrices. This process incorporates both the model’s classification loss and the decision distillation loss between student and teacher models. In phase two, the trained student model’s parameters undergo low-rank decomposition and matrix decomposition, resulting in a decomposed parameter matrix that is uploaded to the server. The reconstruction process involves the inverse processing of these parameters, which are subsequently broadcast from the server to the client.

distillation among student and teacher models. The representation-based part of DDL (\mathcal{L}_{dec-r}) for both teacher and student models are formulated below:

$$\mathcal{L}_{dec-r}^s = \mathcal{L}_{dec}^t = \frac{\mathcal{L}_{rep}}{\mathcal{L}_{task}^t + \mathcal{L}_{task}^s}. \quad (5)$$

In this way, the distillation intensity is weak if the prediction of teacher and student models is incorrect (task losses \mathcal{L}_{task}^t and \mathcal{L}_{task}^s are large). The distillation is highly effective when the teacher and student models are well trained (task losses \mathcal{L}_{task}^t and \mathcal{L}_{task}^s is small), which have the ability to avoid over-fitting and enforcing the extracted latent representation from backbone both teacher and student models toward balance and alignment (have similar knowledge).

In addition, we further introduce decision-based DDL (\mathcal{L}_{dec-d}) that is utilized to distillate the teacher model and student model directly based on their output prediction according to Eq.(4), as follows:

$$\mathcal{L}_{dec-d}^t = \frac{-\sum_i \mathbf{Y}^t \log(\frac{\mathbf{Y}^s}{\mathbf{Y}^t})}{\mathcal{L}_{task}^t + \mathcal{L}_{task}^s}, \quad \mathcal{L}_{dec-d}^s = \frac{-\sum_i \mathbf{Y}^s \log(\frac{\mathbf{Y}^t}{\mathbf{Y}^s})}{\mathcal{L}_{task}^t + \mathcal{L}_{task}^s}, \quad (6)$$

where the term of $-\sum_i \mathbf{Y}^t \log(\frac{\mathbf{Y}^s}{\mathbf{Y}^t})$ and $-\sum_i \mathbf{Y}^s \log(\frac{\mathbf{Y}^t}{\mathbf{Y}^s})$ is the Kullback–Leibler divergence (KLD) often appears in conventional knowledge distillation tasks.

Based on the above-proposed loss function, We can summarize the local loss for both teacher model (denotes \mathcal{L}^t) and student model (denotes \mathcal{L}^s) local optimization as follows:

$$\mathcal{L}^t = \underbrace{\mathcal{L}_{dec-d}^t + \mathcal{L}_{dec-r}^t}_{DDL} + \mathcal{L}_{task}^t, \quad \mathcal{L}^s = \underbrace{\mathcal{L}_{dec-d}^s + \mathcal{L}_{dec-r}^s}_{DDL} + \mathcal{L}_{task}^s, \quad (7)$$

Both the teacher and student models are locally updated using the same optimizers on each client. The student model's gradients \mathbf{g} on the i -th client are calculated as $\mathbf{g}_i^s = \frac{\partial \mathcal{L}_{bik}^s}{\partial \Theta^s}$, where Θ^s represents the student model's parameters. Similarly, the teacher model's gradients on the same client are obtained using $\mathbf{g}_i^t = \frac{\partial \mathcal{L}_{bik}^t}{\partial \Theta^t}$, with Θ^t being the teacher model's parameters.

Once both models are updated, each client transmits student model's parameters Θ^s to the central server. The server employs the FedAvg algorithm [McMahan et al., 2017] to aggregate these parameters into a global model, which it then redistributes to the clients. Subsequently, clients update their student models with the globally aggregated parameters. Concurrently, the local teacher model continues to offer personalized instruction and knowledge transfer. This process repeats until convergence is achieved for both the student and teacher models.

4.3 Global Parameter Decomposition on Global Aggregation

The communication overhead in FL frameworks is largely determined by the volume of parameters transmitted from clients to the server. This overhead poses a significant challenge for systems comprising low-resource devices with limited computational power and communication bandwidth. In resource-constrained environments, increased communication costs and reduced efficiency may compromise the accuracy of decision-making systems. To address this issue, we introduce Global Parameter Decomposition (GPD), a simple yet effective method to compress parameters exchanged during server-client communications. Inspired by low-rank parameter matrix decomposition (LoRA) [Hu et al., 2021], GPD aims to reduce communication costs without sacrificing performance. The locally updated student model parameters are decomposed into two parts:

$$\mathbf{g}_i^s = \mathbf{g}_i^{s,p} \cdot \mathbf{g}_i^{s,n}, \quad \text{where } \mathbf{g}_i^s \in \mathbb{R}^{P \times Q}, \mathbf{g}_i^{s,p} \in \mathbb{R}^{P \times r}, \mathbf{g}_i^{s,n} \in \mathbb{R}^{r \times Q}. \quad (8)$$

For simplicity, we use a two-dimensional representation where the original student model parameters are split into two low-rank matrices, $\mathbf{g}_i^{s,p}$ and $\mathbf{g}_i^{s,n}$, with rank r . We define r as the ratio $Q//P$ (if $Q > P$) or $P//Q$ (if $P > Q$). Prior to uploading, local gradients are decomposed into smaller matrices using singular value decomposition (SVD). The server reconstructs local parameters by multiplying these matrices before aggregation. The aggregated global parameters are then decomposed and sent to clients for reconstruction during model updates. Specifically, we apply SVD to the matrices $\mathbf{g}_i^{s,p}$ and $\mathbf{g}_i^{s,n}$:

$$\mathbf{g}_i^{s,p} \approx U^p \Sigma^p V^p, \quad \mathbf{g}_i^{s,n} \approx U^n \Sigma^n V^n \quad (9)$$

where $U^p \in \mathbb{R}^{Q \times K}$, $\Sigma^p \in \mathbb{R}^{K \times K}$, $V^p \in \mathbb{R}^{K \times r}$, $U^n \in \mathbb{R}^{r \times K}$, $\Sigma^n \in \mathbb{R}^{K \times K}$, $V^n \in \mathbb{R}^{K \times Q}$, and K is the number of retained singular values. In terms of the total number of parameters, if the value of K meets $QK + K^2 + Kr < Pr$ (for $\mathbf{g}_i^{s,p}$), or $rK + K^2 + KQ < Pr$ (for $\mathbf{g}_i^{s,n}$), the uploaded parameter from each client and downloaded parameter from the server can be reduced significantly. In multi-dimensional CNNs utilized in MIC image classification, different parameter matrices (e.g., convolution units, linear layers, etc.) are decomposed independently, and the global parameters on the server are decomposed in the same way. We denote the singular values of $\mathbf{g}_i^{s,p}$ as $[\sigma_1, \sigma_2, \dots, \sigma_r]$, $\mathbf{g}_i^{s,n}$ as $[\sigma_1, \sigma_2, \dots, \sigma_Q]$ ordered by their absolute values. To minimize approximation error, we employ the Variance Explained Criterion [Henseler et al., 2015] to dynamically adjust the number of transmitted singular values, optimizing benefits and minimizing communication overhead in resource-limited environments, as follows:

$$\min_K \frac{\sum_{i=1}^K \sigma_i^2}{\sum_{i=1}^Q \sigma_i^2} > \alpha. \quad (10)$$

This strategy enables clients to transmit parameters with maximum relevant information, preventing the negative effects of unnecessary parameter transmission on model performance and communication costs. The dynamic selection of parameters based on their performance on private client data adds flexibility to the approach. The algorithm implement of FEDMIC is shown in Alg. 1 and Alg. 2.

Algorithm 1 Implement of the proposed FEDMIC

Setting the local learning rate η , client number N , and local dataset $D_i = \{(x_1, y_1), (x_2, y_2), \dots, (x_n, y_n)\}$
Setting communication rounds R , local updating steps e
Setting hyperparameters α ,
for communication rounds $R = 1, 2, 3 \dots$ **do**
 Client-side:
 for each client i in parallel **do**
 Initialize student model Θ_i^s and teacher model Θ_i^t
 $\Theta_i^t \leftarrow \text{LOCALUPDATE}(D_i, \eta, \Theta_i^t / \mathbf{g}_i^t, e)$
 $\Theta_i^s \leftarrow \text{LOCALUPDATE}(D_i, \eta, \Theta_i^s, e)$
 $\mathbf{g}_i^{s,p}, \mathbf{g}_i^{s,n} \leftarrow \text{DECOM}(\mathbf{g}_i^s, e)$
 $U^p \Sigma^p V^p \leftarrow \text{GPD}(\mathbf{g}_i^{s,p}, e)$
 $U^n \Sigma^n V^n \leftarrow \text{GPD}(\mathbf{g}_i^{s,n}, e)$
 Clients upload $U_i^p \Sigma_i^p V_i^p$ and $U_i^n \Sigma_i^n V_i^n$ to the server
 end for
 Server-side:
 Server receives $U^p \Sigma^p V^p$ and $U^n \Sigma^n V^n$
 Server reconstructs \mathbf{g}_i^t
 Server aggregates $\mathbf{g} \leftarrow \sum_i^N \frac{n_i}{n} \mathbf{g}_i^t$
 $\mathbf{g} \leftarrow U \Sigma V$
 Server distribute $\mathbf{g} \leftarrow U \Sigma V$ to each client
end for

Algorithm 2 Implement of LOCALUPDATE

Setting the local student parameter Θ^s , the teacher model parameter Θ^t , and local dataset D .
LocalUpdate(D, η, Θ, e):
for local updating steps $e = 1, 2, 3 \dots$ **do**
 Local model Θ^s and Θ^t trained by private data D
 Compute task losses according to Eq. 4
 Compute representation distillation losses according to Eq. 3
 Compute representation-based decision distillation losses according to Eq. 5
 Compute decision-based decision distillation losses according to Eq. 6
 Compute local losses for both student and teacher models according to Eq. 7
 Parameter update $\Theta^s(\text{new}) \leftarrow \Theta^s(\text{old}), \Theta^t(\text{new}) \leftarrow \Theta^t(\text{old})$
end for

5 Theorems and Proofs

In this work, we actually consider the following distributed optimization model:

$$\min_w \left\{ F(w) = \sum_{k=1}^N p_k F_k(w) \right\} \quad (11)$$

where N is the number of devices, and p_k is the weight of the k -th device such that $p_k \geq 0$ and $\sum_{k=1}^N p_k = 1$. Suppose the k -th device holds the n_k training data: $x_{k,1}, x_{k,2}, \dots, x_{k,n_k}$. The local objective $F_k(\cdot)$ is defined by

$$F_k(w) = \frac{1}{n_k} \sum_{j=1}^{n_k} \mathcal{L}(w; x_{k,j}), \quad (12)$$

where $\mathcal{L}(w; x_{k,j}) := \{\mathcal{L}^t, \mathcal{L}^s\}$
 $:= \{\mathcal{L}_{dec-d}^t + \mathcal{L}_{dec-r}^t + \mathcal{L}_{task}^t, \mathcal{L}_{dec-d}^s + \mathcal{L}_{dec-r}^s + \mathcal{L}_{task}^s\}$

Considering that the student and teacher models are architecturally consistent and updated in parallel during the local update of FEDMIC, we will subsequently consider only the student model's in order to simplify the relevant theorems and proofs, which has no impact on the results.

Theorem 1 (Generalization Bound of FEDMIC). *Consider a on-device medical image classification system with m clients (devices). Let $\mathcal{D}_1, \mathcal{D}_2, \dots, \mathcal{D}_m$ be the true data distribution and $\hat{\mathcal{D}}_1, \hat{\mathcal{D}}_2, \dots, \hat{\mathcal{D}}_m$ be the empirical data distribution. Denote the head h as the hypothesis from \mathcal{H} and d be the VC-dimension of \mathcal{H} . The total number of samples over all clients is N . Then with probability at least $1 - \delta$:*

$$\begin{aligned} & \max_{(\{\mathcal{P}_1\}, \{\mathcal{P}_2\}, \dots, \{\mathcal{P}_m\})} \left| \sum_{i=1}^m \frac{|D_i|}{N} \mathcal{L}_{\mathcal{D}_i}(\theta_i; \cdot) - \sum_{i=1}^m \frac{|D_i|}{N} \mathcal{L}_{\hat{\mathcal{D}}_i}(\theta_i; \cdot) \right| \\ & \leq \sqrt{\frac{N}{2} \log \frac{(m+1)|\mathbf{P}|}{\delta}} + \sqrt{\frac{d}{N} \log \frac{eN}{d}}. \end{aligned} \quad (13)$$

Proof. We start from the McDiarmid's inequality as

$$\mathbb{P}[g(X_1, \dots, X_n) - \mathbb{E}[g(X_1, \dots, X_n)] \geq \epsilon] \leq \exp\left(-\frac{2\epsilon^2}{\sum_{i=1}^n c_i^2}\right) \quad (14)$$

when

$$\sup_{x_1, \dots, x_n} |g(x_1, x_2, \dots, x_n) - g(x_1, x_2, \dots, x_n)| \leq c_i \quad (15)$$

Eq. 15 equals to

$$\mathbb{P}[g(\cdot) - \mathbb{E}[g(\cdot)] \leq \epsilon] \geq 1 - \exp\left(-\frac{2\epsilon^2}{\sum_{i=1}^n c_i^2}\right) \quad (16)$$

which means that with probability at least $1 - \exp\left(-\frac{2\epsilon}{\sum c}\right)$,

$$g(\cdot) - \mathbb{E}[g(\cdot)] \leq \epsilon \quad (17)$$

Let $\delta = \exp\left(-\frac{2\epsilon}{\sum c}\right)$, the above can be rewritten as with the adaptive prompts at least $1 - \delta$,

$$g(\cdot) - \mathbb{E}[g(\cdot)] \leq \sqrt{\frac{\sum_{i=1}^n c_i^2}{2} \log \frac{1}{\delta}} \quad (18)$$

Now we substitute $g(\cdot)$:

$$\max_{(\theta, \theta, \dots, \theta)} \left(\sum_{i=1}^m \frac{|D_i|}{N} \mathcal{L}_{\mathcal{D}}(\theta_i; \cdot) - \sum_{i=1}^m \frac{|D_i|}{N} \mathcal{L}_{\hat{\mathcal{D}}}(\theta_i; \cdot) \right) \quad (19)$$

we can obtain that with probability at least $1 - \delta$, the following holds for specific adaptive prompts,

$$\begin{aligned} & \max_{(\theta, \theta, \dots, \theta)} \left(\sum_{i=1}^m \frac{|D_i|}{N} \mathcal{L}_{\mathcal{D}}(\theta_i; \cdot) - \sum_{i=1}^m \frac{|D_i|}{N} \mathcal{L}_{\hat{\mathcal{D}}}(\theta_i; \cdot) \right) \\ & - \mathbb{E} \left[\max_{(\theta, \theta, \dots, \theta)} \left(\sum_{i=1}^m \frac{|D_i|}{N} \mathcal{L}_{\mathcal{D}}(\theta_i; \cdot) - \sum_{i=1}^m \frac{|D_i|}{N} \mathcal{L}_{\hat{\mathcal{D}}}(\theta_i; \cdot) \right) \right] \\ & \leq \sqrt{\frac{N}{2} \log \frac{1}{\delta}} \end{aligned} \quad (20)$$

Considering there are $(m+1)|\mathbf{P}|$ singular value in total, by using Boole's inequality, with probability at least $1 - \delta$, the following holds,

$$\begin{aligned} & \max_{(\theta, \theta, \dots, \theta)} \left(\sum_{i=1}^m \frac{|D_i|}{N} \mathcal{L}_{\mathcal{D}}(\theta_i; \cdot) - \sum_{i=1}^m \frac{|D_i|}{N} \mathcal{L}_{\hat{\mathcal{D}}}(\theta_i; \cdot) \right) \\ & \leq \mathbb{E} \left[\max_{(\theta, \theta, \dots, \theta)} \left(\sum_{i=1}^m \frac{|D_i|}{N} \mathcal{L}_{\mathcal{D}}(\theta_i; \cdot) - \sum_{i=1}^m \frac{|D_i|}{N} \mathcal{L}_{\hat{\mathcal{D}}}(\theta_i; \cdot) \right) \right] \\ & + \sqrt{\frac{N}{2} \log \frac{(m+1)|\mathbf{P}|}{\delta}} \end{aligned} \quad (21)$$

where N is the total number of samples over all clients.

$$\begin{aligned}
& \mathbb{E} \left[\max_{(\theta, \theta, \dots, \theta)} \left(\sum_{i=1}^m \frac{|D_i|}{N} \mathcal{L}_{\mathcal{D}}(\theta_i; \cdot) - \sum_{i=1}^m \frac{|D_i|}{N} \mathcal{L}_{\hat{\mathcal{D}}}(\theta_i; \cdot) \right) \right] \\
& \leq \mathbb{E} \left[\sum_{i=1}^m \frac{|D_i|}{N} \max_{\{\mathcal{P}\}} \left(\mathcal{L}_{\mathcal{D}}(\theta_i; \cdot) - \mathcal{L}_{\hat{\mathcal{D}}}(\theta_i; \cdot) \right) \right] \\
& \leq^a \sum_{i=1}^m \frac{|D_i|}{N} \mathcal{R}(\mathcal{H}) \\
& \leq \sum_{i=1}^m \frac{|D_i|}{N} \sqrt{\frac{d}{|D_i|} \log \frac{e|D_i|}{d}} \\
& \leq \sum_{i=1}^m \frac{D_i}{N} \sqrt{\frac{d}{|D_i|} \log \frac{eN}{d}} \\
& \leq^b \sqrt{\frac{d}{N} \log \frac{eN}{d}}
\end{aligned} \tag{22}$$

where \mathcal{H} is the hypothesis set of head h , d is the VC-dimension of \mathcal{H} . The a follow from the definition of Rademacher complexity

$$\mathcal{R}_n(\mathcal{F}) = \mathbb{E}_{\sigma} \left[\sup_{f \in \mathcal{F}} \frac{1}{n} \sum_{i=1}^n \sigma_i f(x_i) \right], \tag{23}$$

where $\sigma_1, \sigma_2, \dots, \sigma_n$ are independent Rademacher random variables that take values in $\{-1, 1\}$ with equal probability, \mathbb{E}_{σ} denotes the expectation over the Rademacher variables, x_1, x_2, \dots, x_n are the input data points, and the b follows from Jensen's inequality, so

$$\begin{aligned}
& \max_{(\theta, \theta, \dots, \theta)} \left| \sum_{i=1}^m \frac{|D_i|}{N} \mathcal{L}_{\mathcal{D}}(\theta_i; \cdot) - \sum_{i=1}^m \frac{|D_i|}{N} \mathcal{L}_{\hat{\mathcal{D}}}(\theta_i; \cdot) \right| \\
& \leq \sqrt{\frac{N}{2} \log \frac{(m+1)|\mathcal{P}|}{\delta}} + \sqrt{\frac{d}{N} \log \frac{eN}{d}}
\end{aligned} \tag{24}$$

6 Experiments and Results

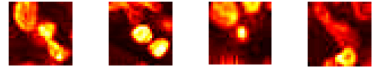
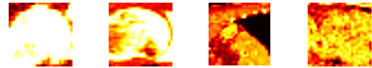
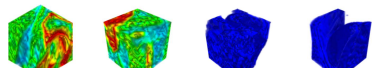
In this section, we describe the dataset and the experimental setup. We then present the results conducted in Non-IID settings. These include standard experiment reports, ablation studies on key components, assessments of parameter impacts, and experiments on differential privacy.

6.1 Dataset and Pre-Processing

Our experiments utilized four representative Medical Image Classification (MIC) datasets derived from the publicly available MedMNIST: BloodMNIST, TissueMNIST, OrganMNIST(2D), and OrganMNIST(3D). These datasets are publicly available at <https://medmnist.com/>. All images were resized to a standard 64×64 resolution. To simulate the data distribution across different clients in federated learning, we partitioned the images into 20 distinct subsets. For each subset (client), data was divided into training, testing, and validation sets in a 7:2:1 ratio. Specific information about the datasets such as the number of samples, some sample examples can be found in **Table 1**.

To demonstrate the effectiveness of our proposed FEDMIC in real-world non-IID scenarios, we simulated a typical FL scenario by assigning each client's data according to a Dirichlet distribution [Wu et al., 2023], specifically expressed as $\mathbf{q} \sim \text{Dirichlet}(\lambda \mathbf{p})$. Here, \mathbf{p} represents the prior class distribution, and λ is a factor that modulates the degree of non-IID characteristics. A larger λ value signifies more pronounced class imbalances within each client, leading to more demanding local tasks characterized by a greater variety of classes and fewer samples per class. As λ increases, inter-client data distribution discrepancies decrease, while intra-client data distribution diversity increases. This

Table 1: Detailed information of the datasets used as well as schematic diagrams including BloodMNIST, TissueMNIST, OrganMNIST2D and OrganMNIST3D. Under FL framework, we assigned them to 20, 20, 20, and 10 clients to simulate Non-IID in real-world applications, respectively.

Dataset	Num. of Class	Num. of Sample	Num. of Client	Examples (four randomly sampled)
BloodMNIST	8	17,092	20	
TissueMNIST	8	236,386	20	
OrganMNIST (2D)	11	25,211	20	
OrganMNIST (3D)	11	1,742	10	

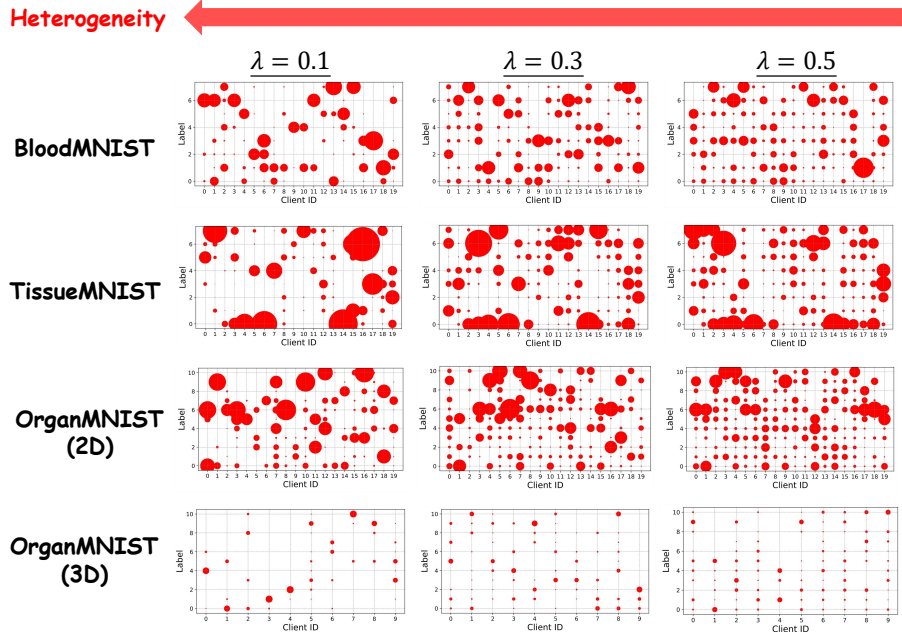


Figure 3: Visualization of four datasets distribution in different degrees of Non-IID environments. From top to bottom are BloodMNIST, TissueMNIST, OrganMNIST (2D) and OrganMNIST (2D), and from left to right are the Dirichlet distribution parameters $\lambda \in \{0.1, 0.3, 0.5\}$. The smaller λ is, the stronger the data Non-IID between clients. In addition, a larger red circle means that the client has more such samples, and the opposite means that there are fewer such samples on the client.

setup rigorously tests the robustness of methods against complex non-IID conditions. We conducted experiments using three Dirichlet parameters, $\lambda \in \{0.1, 0.3, 0.5\}$, to assess the impact of varying degrees of non-IID scenarios. The distribution of client data at different degrees of Non-IID is shown in Figure 3.

6.2 Baselines

We have selected the well-known SOTA FL algorithms, including a personalized algorithm based on parameter localized (FEDBN), based on local regularization (PERFEDAVG), based on knowledge distillation (FEDBE), and FEDALA as the baseline, to demonstrate the superiority of our FEDMIC in MIC classification task. Detailed information of these baselines is as follows:

LOCAL. In the absence of a distributed learning environment, medical images are processed independently by individual clients, precluding any information exchange between them.

FEDAVG. [McMahan et al., 2017] Aggregating local models to obtain a global model via classic average strategy while preserving the privacy of each individual’s data.

FEDBN. [Li et al., 2021b] A personalized FL approach that personalized batch-norm layers in local models and shares remaining parameters globally to achieve highly customized models for each client.

PERFEDAVG. [T Dinh et al., 2020] A personalized FL approach that adapts the global model to each user’s local data distribution while taking into account the similarity between users to improve model generalization.

FEDBE. [Chen and Chao, 2021] A personalized FL approach using Bayesian model integration for robustness in aggregating user predictions and summarizing integrated predictions into global models with the help of knowledge distillation.

FEDALA. [Zhang et al., 2023e] An approach for personalized federated learning that addresses inter-client statistical heterogeneity through its core component, the Adaptive Local Aggregation (ALA) module.

FEDMIC. Our proposed framework introduces Dual Knowledge Distillation (Dual-KD) for local updating and Global Parameter Decomposition (GPD) to achieve a robust global model while maintaining highly customized local models for individual clients under privacy-preserving conditions.

To ensure a fair comparison, we maintained uniform baseline parameters as reported in the original publications. For the local model on each client, we selected **ResNet101** [He et al., 2016]. During training, we configured 50 global communication rounds and 5 local update epochs. We employed SGD as the optimizer, setting the local learning rate to 1×10^{-3} for both teacher and student models. The performance of the framework was evaluated based on accuracy (ACC).

6.3 Main Experiments and Results

In this subsection, we will presents our main experiments on Non-IID environments with different degrees, including $\lambda = 0.1$ (**Table. 2**), $\lambda = 0.3$ (**Table. 3**), and $\lambda = 0.5$ (**Table. 4**). We will analyse the results for three different heterogeneous scenarios with different datasets as the basic unit.

Main Results on $\lambda = 0.1$. The main results is shown in **Table. 2**, which demonstrate that our proposed FEDMIC achieves the best performance across all four datasets and participation rate settings, significantly outperforming the baselines. **(1) BloodMNIST:** FEDMIC achieves 92.13%, 94.84% and 95.11% accuracy at 10%, 30% and 50% participation rates, respectively. Compared to the second best method (FedALA at 10% participation rate, 81.79%), FEDMIC achieved a relative performance improvement of 12.6%. At 50% participation rate, FEDMIC improved accuracy by 4.2% relative to FedALA (91.26%). **(2) TissueMNIST:** FEDMIC achieves accuracies of 64.28%, 69.90%, and 75.83% at different participation rates. At a 10% participation rate, FEDMIC improves performance by 23.3% compared to the second-best method, FedBE (52.12%). At a 50% participation rate, FEDMIC improves accuracy by 10.1% compared to FedALA (68.88%). **(3) OrganMNIST (2D):** FEDMIC achieves 85.55% accuracy at a 50% participation rate, an 8.5% improvement over the second-best method (Local, 78.82%). At a 10% participation rate, FEDMIC (70.21%) achieves a 7.2% improvement relative to FedALA (65.47%). **(4) OrganMNIST (3D):** The advantages of FEDMIC are even more pronounced. It achieves an accuracy of 94.62% at a 50% participation rate, a 6.6% improvement relative to the second-best method (Local, 88.79%). At a 10% participation rate, FEDMIC (76.62%) improves accuracy by 15% over FedALA (66.64%).

Main Results on $\lambda = 0.3$. The main results is shown in **Table. 3**. **(1) BloodMNIST:** FEDMIC performed exceptionally well, achieving the best performance at all participation rates. Notably, at a low participation rate of 10%, FEDMIC achieved an accuracy of 92.56%, an improvement of 27.5% compared to the second-best method (Local, 72.57%), demonstrating its significant advantage in low participation rate scenarios. Compared to the case of $\lambda = 0.1$, FEDMIC’s performance on this dataset slightly improves, particularly at a 30% participation rate, where the accuracy increases from 94.84% to 96.84%. **(2) TissueMNIST:** FEDMIC also maintained its leadership position, achieving

Table 2: Experimental results of the proposed FEDMIC and baseline for four MIC datasets with $\lambda = 0.1$ and client participant ratio $r \in \{10\%, 30\%, 50\%\}$, where **Bold** are the best, and underline represent the second best.

DATASET	BloodMNIST			TissueMNIST			OrganMNIST (2D)			OrganMNIST (3D)		
Method/Ratio	10%	30%	50%	10%	30%	50%	10%	30%	50%	10%	30%	50%
FEDAVG	49.92	58.12	60.23	44.37	52.55	58.75	59.82	64.05	69.92	55.17	61.92	62.35
	± 1.86	± 0.57	± 1.71	± 1.24	± 1.95	± 1.12	± 0.33	± 0.75	± 0.17	± 1.43	± 0.04	± 1.58
LOCAL	68.35	88.32	<u>92.85</u>	57.49	59.85	66.61	<u>69.23</u>	<u>76.42</u>	<u>78.82</u>	68.47	<u>86.18</u>	<u>88.79</u>
	± 1.93	± 1.23	± 0.39	± 2.76	± 0.64	± 1.05	± 1.37	± 0.84	± 2.14	± 1.46	± 1.61	± 2.05
FEDBN	79.28	82.45	87.69	58.55	<u>64.35</u>	67.82	66.12	71.49	75.37	58.24	72.64	76.18
	± 1.47	± 2.51	± 0.09	± 0.81	± 2.26	± 0.45	± 1.11	± 1.14	± 1.87	± 2.64	± 0.87	± 2.32
PERFEDAVG	77.81	87.32	90.55	54.22	60.88	64.85	63.47	72.15	74.28	62.19	78.74	81.12
	± 1.19	± 0.93	± 0.64	± 1.68	± 2.75	± 0.51	± 0.82	± 0.23	± 0.54	± 1.96	± 1.10	± 0.37
FEDBE	81.24	88.21	89.07	52.12	63.43	67.90	63.64	69.52	74.22	64.41	78.55	84.20
	± 1.90	± 0.88	± 1.46	± 1.13	± 0.77	± 2.10	± 1.17	± 1.27	± 1.21	± 1.37	± 1.26	± 1.21
FEDALA	<u>81.79</u>	<u>89.47</u>	<u>91.26</u>	<u>59.11</u>	<u>64.00</u>	<u>68.88</u>	65.47	70.15	76.02	<u>66.64</u>	76.31	83.21
	± 0.42	± 0.61	± 0.54	± 0.58	± 0.04	± 0.17	± 0.62	± 1.47	± 0.66	± 1.07	± 0.44	± 1.62
FEDMIC (Ours)	92.13	94.84	95.11	64.28	69.90	75.83	70.21	77.42	85.55	76.62	87.18	94.62
	± 1.46	± 0.27	± 1.73	± 0.78	± 0.42	± 1.12	± 0.62	± 0.19	± 0.98	± 1.46	± 0.46	± 0.99

accuracies of 66.12%, 70.37%, and 77.27% at various participation rates. Although the advantage over other methods is less pronounced than on BloodMNIST, FEDMIC still performs best at all participation rates. Compared to $\lambda = 0.1$, FEDMIC shows a small improvement in performance on this dataset, specifically from 75.83% to 77.27% at 50% participation rate. **(3) OrganMNIST (2D):** The performance of FEDMIC fluctuated slightly. While it still performs best at 10% and 30% participation, achieving 73.64% and 80.12 per cent accuracy, respectively, the Local method (82.99%) slightly outperforms FEDMIC (86.96%) at 50% participation. **(4) FEDMIC** again maintains the best performance at all participation rates, achieving 79.21%, 89.00%, and 95.85% accuracy, respectively. Compared to $\lambda = 0.1$, FEDMIC’s performance on this dataset improves significantly, especially from 76.62% to 79.21% at a 10% participation rate. At a 10% participation rate, FEDMIC improves its performance by 9.6% relative to the second-best method, Local (72.26%), further proving its superiority in low participation rate scenarios.

Table 3: Experimental results of the proposed PRFL and baseline for four MIC datasets with $\lambda = 0.3$ and client participant ratio $r \in \{10\%, 30\%, 50\%\}$, where **Bold** are the optimal results, and underline represent suboptimal result.

DATASET	BloodMNIST			TissueMNIST			OrganMNIST (2D)			OrganMNIST (3D)		
Method/Ratio	10%	30%	50%	10%	30%	50%	10%	30%	50%	10%	30%	50%
FEDAVG	51.85	60.90	63.09	46.48	56.64	62.22	61.93	68.56	71.91	58.76	65.36	66.28
	± 1.20	± 0.66	± 1.79	± 0.52	± 1.33	± 0.85	± 1.09	± 0.97	± 0.31	± 1.50	± 0.44	± 0.76
LOCAL	72.57	<u>94.90</u>	<u>95.78</u>	60.63	67.16	71.50	75.57	84.99	82.99	<u>72.26</u>	93.39	<u>94.35</u>
	± 1.24	± 0.95	± 1.52	± 0.25	± 1.03	± 0.89	± 1.76	± 0.42	± 1.68	± 0.57	± 1.00	± 0.83
FEDBN	82.46	87.26	93.29	62.23	<u>70.43</u>	73.66	70.45	77.31	82.00	60.92	80.68	84.50
	± 1.02	± 0.23	± 1.39	± 0.17	± 1.90	± 0.56	± 1.07	± 1.68	± 0.82	± 1.57	± 0.73	± 0.48
PERFEDAVG	81.52	90.94	91.62	58.90	65.37	70.48	69.35	<u>81.08</u>	<u>83.33</u>	70.39	87.30	87.74
	± 0.12	± 1.66	± 0.77	± 1.83	± 1.21	± 0.34	± 1.45	± 0.89	± 0.58	± 1.11	± 0.99	± 1.74
FEDBE	<u>83.25</u>	89.62	90.88	62.52	65.58	<u>74.90</u>	67.21	73.80	78.42	67.91	79.19	85.23
	± 0.56	± 1.37	± 0.85	± 0.33	± 1.94	± 0.20	± 1.26	± 1.50	± 0.65	± 1.88	± 0.91	± 0.44
FEDALA	82.95	89.63	92.46	<u>64.03</u>	67.29	70.69	<u>74.07</u>	74.62	79.90	70.69	79.02	85.13
	± 1.57	± 0.24	± 1.32	± 0.02	± 0.75	± 1.98	± 0.37	± 1.11	± 0.90	± 0.65	± 1.79	± 0.14
FEDMIC (Ours)	92.56	96.84	96.41	66.12	70.37	77.27	73.64	80.12	86.96	79.21	<u>89.00</u>	95.85
	± 1.27	± 0.33	± 1.90	± 0.57	± 1.64	± 0.68	± 1.02	± 0.45	± 1.78	± 1.05	± 0.12	± 0.96

Main Results on $\lambda = 0.5$. The results is shown in **Table 4**. **(1) BloodMNIST:** FEDMIC again maintains the best performance at all participation rates, achieving 79.21%, 89.00%, and 95.85% accuracy, respectively. Compared to $\lambda = 0.1$, FEDMIC’s performance on this dataset improves significantly, especially from 76.62% to 79.21% at 10% participation rate. At 10% participation rate, FEDMIC improves its performance by 9.6% relative to the second best method, Local (72.26%), again proving its superiority in low participation rate scenarios. **(2) TissueMNIST:** FEDMIC performed best at 30% and 50% participation rates, achieving 73.12% and 79.12% accuracy, respectively. At 10%

participation rate, FEDMIC remains competitive although its accuracy (67.18%) is slightly lower than FedALA (69.67%). **(3) OrganMNIST (2D):** FEDMIC performed best at 10% and 30% participation rates, achieving 74.49% and 83.11% accuracy, respectively. At 50% participation rate, although FEDMIC (89.24%) is slightly lower than the Local method (88.25%), it still outperforms the other methods. This result is similar to the case of $\lambda = 0.3$, suggesting that a high participation rate may make simple local training more effective under some specific data distributions. **(4) OrganMNIST (3D):** FEDMIC again maintains the best performance at all participation rates, achieving 81.04%, 89.48%, and 96.33% accuracy, respectively. Compared to $\lambda = 0.3$, FEDMIC’s performance on this dataset shows further improvement, especially at high participation rates. At 10% participation rate, FEDMIC improves its performance by 4.4% relative to the second best method, Local (77.65%), again proving its superiority in low participation rate scenarios.

Table 4: Experimental results of our FEDMIC and baseline for four MIC datasets with $\lambda = 0.5$ and client participant ratio $r \in \{10\%, 30\%, 50\%\}$, where **Bold** are the optimal results, and underline represent suboptimal result.

DATASET	BloodMNIST			TissueMNIST			OrganMNIST (2D)			OrganMNIST (3D)		
	Method/Ratio	10%	30%	50%	10%	30%	50%	10%	30%	50%	10%	30%
FEDAVG	56.45 ± 1.34	64.48 ± 0.87	68.68 ± 1.12	47.26 ± 0.65	60.53 ± 1.56	63.32 ± 1.43	64.21 ± 0.98	74.99 ± 1.75	76.23 ± 0.29	59.08 ± 1.68	68.41 ± 0.52	71.23 ± 1.21
LOCAL	77.92 ± 1.03	<u>96.18</u> ± 1.68	<u>96.37</u> ± 0.86	65.69 ± 1.01	75.30 ± 1.29	<u>76.48</u> ± 1.74	77.72 ± 0.58	86.28 ± 1.20	<u>88.25</u> ± 1.02	<u>77.65</u> ± 0.77	94.56 ± 1.31	<u>95.21</u> ± 1.91
FEDBN	83.51 ± 1.94	89.52 ± 1.23	93.01 ± 1.41	67.13 ± 0.06	68.06 ± 1.11	73.68 ± 0.57	73.23 ± 1.12	76.28 ± 1.76	82.22 ± 0.98	71.92 ± 1.81	76.27 ± 1.27	83.93 ± 1.54
PERFEDAVG	82.30 ± 1.12	91.36 ± 0.68	91.55 ± 1.57	61.31 ± 0.99	<u>68.23</u> ± 1.40	72.68 ± 1.15	71.95 ± 0.86	76.21 ± 1.34	81.77 ± 0.72	70.01 ± 1.08	80.55 ± 0.53	88.32 ± 1.66
FEDBE	84.12 ± 1.01	90.10 ± 1.87	91.94 ± 0.56	<u>68.94</u> ± 1.18	69.20 ± 0.33	73.27 ± 1.90	68.45 ± 0.82	75.58 ± 1.60	81.79 ± 0.44	69.62 ± 1.35	80.38 ± 0.68	86.61 ± 1.75
FEDALA	84.20 ± 1.45	90.00 ± 0.88	92.99 ± 1.12	69.67 ± 0.64	70.60 ± 1.29	73.31 ± 0.73	<u>75.33</u> ± 1.01	76.28 ± 0.92	82.62 ± 1.54	73.22 ± 0.46	81.27 ± 1.67	87.12 ± 0.53
FEDMIC (Ours)	93.42 ± 1.45	96.99 ± 1.21	97.97 ± 0.98	67.18 ± 0.62	<u>73.12</u> ± 1.30	79.12 ± 1.88	74.49 ± 1.15	<u>83.11</u> ± 0.89	89.24 ± 0.34	81.04 ± 1.73	89.48 ± 0.47	96.33 ± 1.60

General Analysis and Discussion. Based on the above quantitative analysis for the results at different λ , we can find that: (1) In most cases, FEDMIC demonstrates superior performance to other benchmark methods. This advantage is demonstrated for different datasets, participation rates and λ values, proving the robustness and adaptability of the FEDMIC. In particular, FEDMIC consistently leads in scenarios dealing with low participation rates, showing its superior performance in federated learning environments with limited client participation. (2) For all values of λ , the performance of FEDMIC generally shows an upward trend as the participation rate increases (from 10% to 50%). This suggests that FEDMIC is able to effectively utilise more client data to improve model performance, while also maintaining its advantages at low participation rates. (3) Despite fluctuating performance under different conditions, FEDMIC generally showed good stability and consistency. In conclusion, the superiority of FEDMIC under different medical image classification datasets comes from the dual knowledge distillation mechanism and global parameter decomposition mechanism in which we propose. The former provides powerful global knowledge to the local student model while also providing it with personalised insights into the local data, and each client storing heterogeneous medical image data is provided with an independent and highly personalised model, which is superior to training a separate model for each client because our framework breaks down the data silos and facilitates knowledge fusion. In addition, the latter provides a lightweight filtering strategy for the global aggregation process, which avoids bias in global knowledge by decomposing client parameters and retaining as much valid information as possible. These two mechanisms complement each other and further enhance the performance of our FEDMIC in different tasks and scenarios.

6.4 Hyperparameter Sensitivity

We examined the impact of parameter α on FEDMIC performance using the Global Parameter Decomposition strategy. Three additional values ($\alpha \in \{0.90, 0.92, 0.95\}$) were tested alongside the standard value of $\alpha = 0.98$ across four datasets. **Table 5** presents the results, which indicate that $\alpha = 0.98$ yields optimal performance. Lower α values resulted in reduced effectiveness due

to insufficient parameter exchange between client and server, leading to loss of critical information. Conversely, higher values led to excessive exchange, introducing superfluous information.

Table 5: Experimental results on the performance with different $\alpha \in \{0.90, 0.92, 0.95, 0.98\}$, where **Bold** denotes the best, Underline denotes the second best. $\alpha = 0.98$ was the original setting.

α	BloodMNIST	TissueMNIST	OrganMNIST (2D)	OrganMNIST (3D)
0.98	93.42 ± 1.45	67.18 ± 0.62	74.49 ± 1.15	81.04 ± 1.73
0.90	92.11 ± 0.46	<u>66.91</u> ± 0.18	73.59 ± 1.22	80.16 ± 0.21
0.92	<u>92.49</u> ± 1.46	<u>67.04</u> ± 0.82	73.26 ± 1.02	80.00 ± 1.72
0.95	91.21 ± 1.23	66.20 ± 0.12	<u>74.04</u> ± 1.22	81.22 ± 0.40

6.5 Ablation Studies

We demonstrate the effectiveness and the necessity of the important components of our method through a series of ablation studies. Our FEDMIC’s key innovations are in knowledge distillation and parameter decomposition, so we conduct ablation studies from two perspectives: (1) KD-based Ablation and (2) Parameter Decomposition-based Ablation. Here’s the detailed setup for them:

KD-based Ablation We evaluate the impact of our dual knowledge distillation mechanism by conducting experiments without certain parts:

- FEDMIC-A: This version omits the Distillation Auxiliary Matrix for local models. The correction loss is simply the MSE: $\mathcal{L}_{rep} = \frac{1}{n} \sum_{i=1}^n (\mathbf{H}_{hs}^s - \mathbf{H}_{hs}^t)$.
- FEDMIC-B: This version removes the representation-based DDL. The local loss is defined as $\mathcal{L}^t = \mathcal{L}_{dec-d}^t + \mathcal{L}_{task}^t$ and $\mathcal{L}^s = \mathcal{L}_{dec-d}^s + \mathcal{L}_{task}^s$ for the local teacher and student models, respectively. *Why representation-based DDL instead of decision-based DDL? The latter encompasses the framework’s critical distillation term, and its removal would substantially compromise the integrity of key procedural steps.*

Parameter Decomposition-based Ablation We explore the effectiveness of our parameter decomposition strategy:

- FEDMIC-C: This scenario removes Global Parameters Decomposition. As a result, full client model parameters are transmitted between clients and the server instead of just a subset of lightweight local model parameters.

Table 6: Comparison of performance under $\lambda = 0.1$, where **Bold** denotes the best performance of incense under KD-based ablation and **Bold** denotes the best result under parameters decomposition-based ablation experiments.

Method / Dataset	BloodMNIST	TissueMNIST	OrganMNIST (2D)	OrganMNIST (3D)
FEDMIC	92.13 ± 1.46	64.28 ± 0.78	70.21 ± 0.62	76.62 ± 1.46
	11.49% of Complete Model Parameters Communication			
FEDMIC-A	90.44 ± 0.12	61.03 ± 0.45	66.92 ± 0.46	73.10 ± 0.63
	11.49% of Complete Model Parameters Communication			
FEDMIC-B	91.00 ± 0.42	60.21 ± 0.12	63.26 ± 1.12	70.82 ± 0.41
	11.49% of Complete Model Parameters Communication			
FEDMIC-C	92.33 ± 0.42	65.29 ± 0.32	69.75 ± 0.19	76.76 ± 0.67
	100% of Complete Model Parameters Communication			

We conducted ablation studies for three scenarios, consistent with previous experiments, to assess FEDMIC at 10% participation rate. These results are presented in Table 6 (for $\lambda = 0.1$), Table 7 (for

Table 7: Comparison of performance under $\lambda = 0.3$, where **Bold** denotes the best performance of incense under knowledge distillation-based ablation experiments and **Bold** denotes the best result under parameters decomposition-based ablation experiments.

Method / Dataset	BloodMNIST	TissueMNIST	OrganMNIST (2D)	OrganMNIST (3D)
FEDMIC	92.56 ± 1.27	66.12 ± 0.57	73.64 ± 1.02	79.21 ± 1.05
	11.49% of Complete Model Parameters Communication			
FEDMIC-A	90.66 ± 0.12	62.24 ± 0.68	68.22 ± 0.24	75.22 ± 0.62
	11.49% of Complete Model Parameters Communication			
FEDMIC-B	91.70 ± 0.43	62.67 ± 0.98	69.05 ± 0.32	72.45 ± 0.29
	11.49% of Complete Model Parameters Communication			
FEDMIC-C	92.22 ± 0.12	67.43 ± 0.87	74.02 ± 0.62	80.20 ± 1.04
	100% of Complete Model Parameters Communication			

Table 8: Comparison of performance under $\lambda = 0.5$, where **Bold** denotes the best performance of incense under knowledge distillation-based ablation experiments and **Bold** denotes the best result under parameters decomposition-based ablation experiments.

Method / Dataset	BloodMNIST	TissueMNIST	OrganMNIST (2D)	OrganMNIST (3D)
FEDMIC	93.42 ± 0.43	67.18 ± 0.24	74.49 ± 0.65	87.04 ± 0.23
	11.49% of Complete Model Parameters Communication			
FEDMIC-A	90.62 ± 0.42	63.21 ± 0.16	69.36 ± 0.20	81.00 ± 1.12
	11.49% of Complete Model Parameters Communication			
FEDMIC-B	91.23 ± 0.21	63.34 ± 0.54	69.89 ± 0.42	79.33 ± 0.56
	11.49% of Complete Model Parameters Communication			
FEDMIC-C	93.90 ± 0.22	68.12 ± 0.89	75.21 ± 0.73	88.04 ± 0.48
	100% of Complete Model Parameters Communication			

$\lambda = 0.3$), and Table 8 and (for $\lambda = 0.5$). From these tables, we observed that: **(1)** In the KD-based ablation, standard FEDMIC beats FEDMIC-A and FEDMIC-B. This indicates a drop in performance *without the Auxiliary Matrix and Representation-based DDL*, highlighting their importance in our FEDMIC; **(2)** For the parameter decomposition-based ablation, FEDMIC-C, which sends full model parameters, increased the data exchange by about 88.51%, leading to more communication overhead and reduced efficiency. The performance gains were marginal or even negative, showing that transmitting an additional **88.51%** of parameters is not cost-effective; In summary, these ablation studies confirm the significance and effectiveness of each component in our FEDMIC.

6.6 Differential Privacy

To further safeguard healthcare organization privacy in the proposed FEDMIC, we implement differential privacy (DP) [Dwork, 2006] by adding random Gaussian noise to the model’s gradients during global aggregation, as suggested by [Chen et al., 2023c]. We evaluated the performance of FEDMIC both with and without DP. The noise, scaled by a factor τ , is added to the shared parameters. We tested τ values of $\{1e^{-3}, 1e^{-2}, 5e^{-2}\}$ to apply differential privacy at varying levels in FEDMIC and compared it with the standard FedAvg.

Table 9: Results of Differential Privacy experiments (DP factor $\tau \in \{1e^{-3}, 1e^{-2}, 5e^{-2}\}$) of the proposed FEDMIC and baseline methods under four fine-grained classification datasets under the Dirichlet Non-IID setting ($\lambda = 0.1$), where **Bold** denotes the optimal result, Underline denotes the suboptimal result, \downarrow denotes the degradation of the performance, with lower being better. Note that *w* and *wo* present *with* and *without*, respectively.

METHOD	DIFFERENTIAL PRIVACY	BloodMNIST	TissueMNIST	OrganMNIST (2D)	OrganMNIST (3D)
FEDAVG	<i>wo</i>	49.92 \pm 1.86	44.37 \pm 1.24	59.82 \pm 0.33	55.17 \pm 1.43
	<i>w</i> ($\tau = 1e^{-3}$)	46.83 \pm 0.75	41.95 \pm 0.62	56.59 \pm 0.42	52.44 \pm 1.40
	<i>w</i> ($\tau = 1e^{-2}$)	43.78 \pm 0.42	39.52 \pm 0.62	54.31 \pm 0.19	50.16 \pm 0.29
	<i>w</i> ($\tau = 5e^{-2}$)	39.96 \pm 0.56	34.83 \pm 0.63	51.24 \pm 0.11	45.62 \pm 0.31
	Mean Variation	6.40 \downarrow	5.60 \downarrow	5.77 \downarrow	5.76 \downarrow
FedMIC (Ours)	<i>wo</i>	92.13 \pm 1.46	64.28 \pm 0.78	70.21 \pm 0.62	76.62 \pm 1.46
	<i>w</i> ($\tau = 1e^{-3}$)	90.87 \pm 0.71	62.69 \pm 0.21	68.53 \pm 0.45	74.95 \pm 0.12
	<i>w</i> ($\tau = 1e^{-2}$)	89.45 \pm 0.33	61.32 \pm 1.21	67.08 \pm 1.09	73.41 \pm 1.32
	<i>w</i> ($\tau = 5e^{-2}$)	87.92 \pm 1.27	59.76 \pm 0.42	65.47 \pm 0.26	71.83 \pm 0.10
	Mean Variation	4.21 \downarrow	4.52 \downarrow	4.74 \downarrow	4.79 \downarrow

Table 9 presents the performance of *FedMIC* and baseline methods on four fine-grained classification datasets under the Non-IID setting with $\lambda = 0.1$ and a client participation rate of 10%. The results indicate a slight decrease in *FedMIC*'s performance after implementing DP. Nevertheless, *FedMIC* continues to outperform standard FedAvg across all four datasets. As *FedMIC* only transmits a subset of parameters during client-server communication, adding noise to these parameters suffices to maintain privacy security. Moreover, the performance degradation due to DP is less pronounced for FedMIC compared to baseline methods that exchange full model parameters during client-server communication.

Additional Discussion about Privacy FL can be vulnerable to data breaches even when data is not directly shared among clients during global model training. An attacker might infer the original data from client-sent gradients, especially with small batch sizes and local training steps. Our FEDMIC approach mitigates this risk by employing a local model for each participant, comprising teacher and student models for private data training. We implement a cost-effective parameter decomposition strategy during client-server communication, transmitting only a subset of parameters. This approach impedes attackers' ability to reconstruct original data from partial gradients. Furthermore, we enhance the strategy with adjustable control coefficients α , further complicating potential inference attacks on raw data, even as the number of training rounds approaches infinity: $e \rightarrow \infty$.

7 Conclusion and Future Works

This paper introduces a novel privacy-preserving framework for medical image classification (FEDMIC), combining dual knowledge distillation (**Dual-KD**) with global parameter decomposition (**GPD**). The Dual-KD enables clients to leverage a rich global knowledge base, enhancing personalized representation of local data and offering a robust, customized solution for varied environments. The GPD strategy reduces communication costs by requiring participants to upload only select parameters rather than entire models, particularly beneficial in resource-constrained settings. Extensive evaluation on real-world medical image classification (including 2D and 3D) datasets confirms the effectiveness and advantages of our proposed FEDMIC.

Limitations Our work has two main limitations: (1) Training both student and teacher models on each client can strain local resources, especially with large models, and (2) The effectiveness of the low-rank decomposition process in reducing upload size may diminish when student model parameter dimensions across clients are not widely separated or consistent.

Future Work Future research will focus on two areas: (1) **Framework level:** We aim to further reduce client-server communication costs while maintaining high performance in real-world medical imaging applications and (2) **Application level:** We plan to extend the framework to a wider range of applications, particularly in visual language tasks, including multimodal medical data retrieval and fusion. Our goal is to develop cost-effective solutions for AI-related medical applications in resource-constrained environments.

References

- Shengchao Chen, Sufen Ren, Guanjun Wang, Mengxing Huang, and Chenyang Xue. Interpretable cnn-multilevel attention transformer for rapid recognition of pneumonia from chest x-ray images. *IEEE Journal of Biomedical and Health Informatics*, 2023a.
- Jiaying Shi, Shengchao Chen, Benguo Yu, Yi Ren, Guanjun Wang, and Chenyang Xue. Recognition system for diagnosing pneumonia and bronchitis using children’s breathing sounds based on transfer learning. *Intelligent Automation & Soft Computing*, 37(3), 2023.
- Hao Li, Chengcheng Li, Jian Wang, Aimin Yang, Zezhong Ma, Zunqian Zhang, and Dianbo Hua. Review on security of federated learning and its application in healthcare. *Future Generation Computer Systems*, 144: 271–290, 2023.
- Meirui Jiang, Holger R Roth, Wenqi Li, Dong Yang, Can Zhao, Vishwesh Nath, Daguang Xu, Qi Dou, and Ziyue Xu. Fair federated medical image segmentation via client contribution estimation. In *Proceedings of the IEEE/CVF Conference on Computer Vision and Pattern Recognition*, pages 16302–16311, 2023.
- Jiahao Wang, Hong Peng, Shengchao Chen, and Sufen Ren. Ensemble learning for retinal disease recognition under limited resources. *Medical & Biological Engineering & Computing*, pages 1–14, 2024a.
- Brendan McMahan, Eider Moore, Daniel Ramage, Seth Hampson, and Blaise Agueria y Arcas. Communication-efficient learning of deep networks from decentralized data. In *Artificial intelligence and statistics*, pages 1273–1282. PMLR, 2017.
- K Dasaradharami Reddy, Thippa Reddy Gadekallu, et al. A comprehensive survey on federated learning techniques for healthcare informatics. *Computational Intelligence and Neuroscience*, 2023, 2023.
- Mubashir Imran, Hongzhi Yin, Tong Chen, Quoc Viet Hung Nguyen, Alexander Zhou, and Kai Zheng. Refrs: Resource-efficient federated recommender system for dynamic and diversified user preferences. *ACM Transactions on Information Systems*, 41(3):1–30, 2023.
- Shijie Zhang, Wei Yuan, and Hongzhi Yin. Comprehensive privacy analysis on federated recommender system against attribute inference attacks. *IEEE Transactions on Knowledge and Data Engineering*, 2023a.
- Honglei Zhang, Fangyuan Luo, Jun Wu, Xiangnan He, and Yidong Li. Lightfr: Lightweight federated recommendation with privacy-preserving matrix factorization. *ACM Transactions on Information Systems*, 41(4): 1–28, 2023b.
- Shengchao Chen, Guodong Long, Tao Shen, and Jing Jiang. Prompt federated learning for weather forecasting: Toward foundation models on meteorological data. *arXiv preprint arXiv:2301.09152*, 2023b.
- Shengchao Chen, Guodong Long, Tao Shen, Tianyi Zhou, and Jing Jiang. Spatial-temporal prompt learning for federated weather forecasting. *arXiv preprint arXiv:2305.14244*, 2023c.
- Zhiwei Zhai, Qiong Wu, Shuai Yu, Rui Li, Fei Zhang, and Xu Chen. Fedleo: An offloading-assisted decentralized federated learning framework for low earth orbit satellite networks. *IEEE Transactions on Mobile Computing*, 2023.
- Xiaokang Zhang, Boning Zhang, Weikang Yu, and Xudong Kang. Federated deep learning with prototype matching for object extraction from very-high-resolution remote sensing images. *IEEE Transactions on Geoscience and Remote Sensing*, 61:1–16, 2023c.
- Shengchao Chen, Xinchun Wang, Sufen Ren, Jianli Yang, Yaqian Zhang, and Guanjun Wang. Collaborative photonic crystal fiber property optimization: A new paradigm for reverse design. *IEEE Photonics Technology Letters*, 2023d.
- Sufen Ren, Shengchao Chen, Jiahao Wang, Haoyang Xu, Xuan Hou, Mengxing Huang, Jianxun Liu, and Guanjun Wang. A distributed photonic crystal fiber reverse design framework based on multi-source knowledge fusion. *Optical Fiber Technology*, 84:103718, 2024.
- Xiangzuo Huo, Gang Sun, Shengwei Tian, Yan Wang, Long Yu, Jun Long, Wendong Zhang, and Aolun Li. Hifuse: Hierarchical multi-scale feature fusion network for medical image classification. *Biomedical Signal Processing and Control*, 87:105534, 2024.
- Qi Han, Xin Qian, Hongxiang Xu, Kepeng Wu, Lun Meng, Zicheng Qiu, Tengfei Weng, Baoping Zhou, and Xianqiang Gao. Dm-cnn: Dynamic multi-scale convolutional neural network with uncertainty quantification for medical image classification. *Computers in Biology and Medicine*, 168:107758, 2024.

- Shengchao Chen, Guodong Long, Jing Jiang, Dikai Liu, and Chengqi Zhang. Foundation models for weather and climate data understanding: A comprehensive survey. *arXiv preprint arXiv:2312.03014*, 2023e.
- Shengchao Chen, Ting Shu, Huan Zhao, and Yuan Yan Tang. Mask-cnn-transformer for real-time multi-label weather recognition. *Knowledge-Based Systems*, 278:110881, 2023f.
- Shengchao Chen, Ting Shu, Huan Zhao, Guo Zhong, and Xunlai Chen. Tempee: Temporal-spatial parallel transformer for radar echo extrapolation beyond auto-regression. *arXiv preprint arXiv:2304.14131*, 2023g.
- Hong Peng, Shengchao Chen, Ning Niu, Jiahao Wang, Qiaoyi Yao, Lu Wang, Yixuan Wang, Jurui Tang, Guanjun Wang, Mengxing Huang, et al. Diffusion model in semi-supervised scleral segmentation. In *2023 IEEE 6th International conference on pattern recognition and artificial intelligence (PRAI)*, pages 376–382. IEEE, 2023.
- Shengchao Chen, Sufen Ren, Guanjun Wang, Mengxing Huang, and Chenyang Xue. Cmt: Interpretable model for rapid recognition pneumonia from chest x-ray images by fusing low complexity multilevel attention mechanism. *arXiv preprint arXiv:2210.16584*, 2022a.
- Shengchao Chen, Ting Shu, Huan Zhao, Qilin Wan, Jincan Huang, and Cailing Li. Dynamic multiscale fusion generative adversarial network for radar image extrapolation. *IEEE Transactions on Geoscience and Remote Sensing*, 60:1–11, 2022b.
- Jiahao Wang, Hong Peng, Shengchao Chen, and Sufen Ren. Less is more: Ensemble learning for retinal disease recognition under limited resources. *arXiv preprint arXiv:2402.09747*, 2024b.
- David Neumann, Andreas Lutz, Karsten MÅ1/4ller, and Wojciech Samek. A privacy preserving system for movie recommendations using federated learning. *ACM Transactions on Recommender Systems*, 2023.
- Shengchao Chen, Guodong Long, Jing Jiang, and Chengqi Zhang. Personalized adapter for large meteorology model on devices: Towards weather foundation models. *arXiv preprint arXiv:2405.20348*, 2024.
- Ashish Rauniar, Desta Haileselassie Hagos, Debesh Jha, Jan Erik Håkegård, Ulas Bagci, Danda B Rawat, and Vladimir Vlassov. Federated learning for medical applications: A taxonomy, current trends, challenges, and future research directions. *IEEE Internet of Things Journal*, 2023.
- Lianhong Zhang, Yuxin Wu, Lunyuan Chen, Lisheng Fan, and Arumugam Nallanathan. Scoring aided federated learning on long-tailed data for wireless iomt based healthcare system. *IEEE Journal of Biomedical and Health Informatics*, 2023d.
- Tian Li, Anit Kumar Sahu, Manzil Zaheer, Maziar Sanjabi, Ameet Talwalkar, and Virginia Smith. Federated optimization in heterogeneous networks. *Proceedings of Machine learning and systems*, 2:429–450, 2020.
- Sai Praneeth Karimireddy, Satyen Kale, Mehryar Mohri, Sashank Reddi, Sebastian Stich, and Ananda Theertha Suresh. Scaffold: Stochastic controlled averaging for federated learning. In *International conference on machine learning*, pages 5132–5143. PMLR, 2020.
- Neta Shoham, Tomer Avidor, Aviv Keren, Nadav Israel, Daniel Benditkis, Liron Mor-Yosef, and Itai Zeitak. Overcoming forgetting in federated learning on non-iid data. *arXiv preprint arXiv:1910.07796*, 2019.
- Xin Yao and Lifeng Sun. Continual local training for better initialization of federated models. In *2020 IEEE International Conference on Image Processing (ICIP)*, pages 1736–1740. IEEE, 2020.
- Qinbin Li, Bingsheng He, and Dawn Song. Model-contrastive federated learning. In *Proceedings of the IEEE/CVF conference on computer vision and pattern recognition*, pages 10713–10722, 2021a.
- Jingyi Xu, Zihan Chen, Tony QS Quek, and Kai Fong Ernest Chong. Fedcorr: Multi-stage federated learning for label noise correction. In *Proceedings of the IEEE/CVF Conference on Computer Vision and Pattern Recognition*, pages 10184–10193, 2022.
- Canh T Dinh, Nguyen Tran, and Josh Nguyen. Personalized federated learning with moreau envelopes. *Advances in Neural Information Processing Systems*, 33:21394–21405, 2020.
- Alireza Fallah, Aryan Mokhtari, and Asuman Ozdaglar. Personalized federated learning with theoretical guarantees: A model-agnostic meta-learning approach. *Advances in Neural Information Processing Systems*, 33:3557–3568, 2020.
- Xiaoxiao Li, Meirui Jiang, Xiaofei Zhang, Michael Kamp, and Qi Dou. Fedbn: Federated learning on non-iid features via local batch normalization. *arXiv preprint arXiv:2102.07623*, 2021b.

- Hong-You Chen and Wei-Lun Chao. Fedbe: Making bayesian model ensemble applicable to federated learning, 2021.
- Daliang Li and Junpu Wang. Fedmd: Heterogenous federated learning via model distillation. *arXiv preprint arXiv:1910.03581*, 2019.
- Tao Lin, Lingjing Kong, Sebastian U Stich, and Martin Jaggi. Ensemble distillation for robust model fusion in federated learning. *Advances in Neural Information Processing Systems*, 33:2351–2363, 2020.
- Felix Sattler, Arturo Marban, Roman Rischke, and Wojciech Samek. Communication-efficient federated distillation. *arXiv preprint arXiv:2012.00632*, 2020.
- Zhuangdi Zhu, Junyuan Hong, and Jiayu Zhou. Data-free knowledge distillation for heterogeneous federated learning. In *International conference on machine learning*, pages 12878–12889. PMLR, 2021.
- Sameer Bibikar, Haris Vikalo, Zhangyang Wang, and Xiaohan Chen. Federated dynamic sparse training: Computing less, communicating less, yet learning better. In *Proceedings of the AAAI Conference on Artificial Intelligence*, volume 36, pages 6080–6088, 2022.
- Xin Yao, Tianchi Huang, Chenglei Wu, Rui-Xiao Zhang, and Lifeng Sun. Federated learning with additional mechanisms on clients to reduce communication costs. *arXiv preprint arXiv:1908.05891*, 2019.
- Rong Dai, Li Shen, Fengxiang He, Xinmei Tian, and Dacheng Tao. Dispf: Towards communication-efficient personalized federated learning via decentralized sparse training. *arXiv preprint arXiv:2206.00187*, 2022.
- Gousia Habib, Tausifa Jan Saleem, and Brejesh Lall. Knowledge distillation in vision transformers: A critical review. *arXiv preprint arXiv:2302.02108*, 2023.
- Edward J Hu, Yelong Shen, Phillip Wallis, Zeyuan Allen-Zhu, Yuanzhi Li, Shean Wang, Lu Wang, and Weizhu Chen. Lora: Low-rank adaptation of large language models. *arXiv preprint arXiv:2106.09685*, 2021.
- Jörg Henseler, Christian M Ringle, and Marko Sarstedt. A new criterion for assessing discriminant validity in variance-based structural equation modeling. *Journal of the academy of marketing science*, 43:115–135, 2015.
- Xinghao Wu, Xuefeng Liu, Jianwei Niu, Guogang Zhu, and Shaojie Tang. Bold but cautious: Unlocking the potential of personalized federated learning through cautiously aggressive collaboration. In *Proceedings of the IEEE/CVF International Conference on Computer Vision*, pages 19375–19384, 2023.
- Jianqing Zhang, Yang Hua, Hao Wang, Tao Song, Zhengui Xue, Ruhui Ma, and Haibing Guan. Fedala: Adaptive local aggregation for personalized federated learning. In *Proceedings of the AAAI Conference on Artificial Intelligence*, volume 37, pages 11237–11244, 2023e.
- Kaiming He, Xiangyu Zhang, Shaoqing Ren, and Jian Sun. Deep residual learning for image recognition. In *Proceedings of the IEEE conference on computer vision and pattern recognition*, pages 770–778, 2016.
- Cynthia Dwork. Differential privacy. In *International colloquium on automata, languages, and programming*, pages 1–12. Springer, 2006.